Neutrino physics: Theory and experiment (SS2021)
Neutrinoless double beta decay

Teresa Marrodán Undagoitia

Max-Planck-Institut für Kernphysik,
Saupfercheckweg 1, 69117 Heidelberg, Germany

E-mail: marrodan@mpi-hd.mpg.de

Contents

1. Lecture 7: Neutrinoless double beta decay

Neutrinoless double-beta decay [1] is a nuclear physics process which tests experimentally lepton number violation, and if neutrinos are Majorana particles. This lecture will briefly recap on the motivation to search for this process, discuss the main experimental aspects and summarize current results.

1.1. Introduction

Double-beta decay is a nuclear physics process in which the nuclear charge is changed by two units [2]:

$$(Z, A) \rightarrow (Z + 2, A) + 2e^- + 2\overline{\nu}_e. \tag{1}$$

This process can be seen as two simultaneous neutron decays and takes place for a limited number of isotopes.

The process in equation 1 could hypothetically happen without the emission of neutrinos:

$$(Z, A) \rightarrow (Z + 2, A) + 2e^-. \tag{2}$$

In this case, the **total lepton number is violated** which is forbidden in the Standard Model of particle physics. Figure 1 shows the two neutrino decay ($2\nu\beta\beta$) on the left side and a possibility for the neutrinoless process ($0\nu\beta\beta$) on the right.

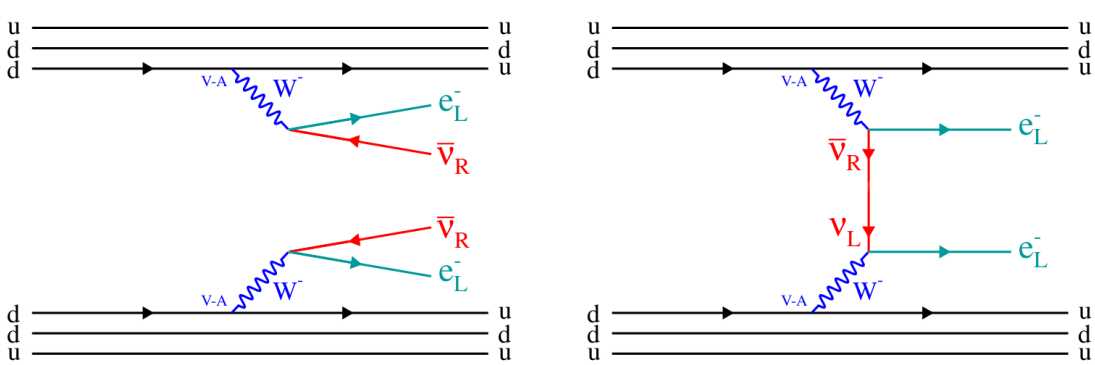

Figure 1. Right: representation of the two neutrino double beta decay. Left: an example of the neutrinoless double beta decay via a virtual exchange of a light Majorana neutrino.

In that example it is assumed that neutrinos are Majorana particles and the neutrino emitted in one of the beta decays would be absorbed in the other. However, the measurement of $0\nu\beta\beta$ just tells that lepton number is violated and not what is the mechanism for the decay.

Figure 2 shows the spectral shape for both equation 1 (dashed black) with a continuous spectrum and for equation 2 (blue) where a monoenergetic signal is produced.

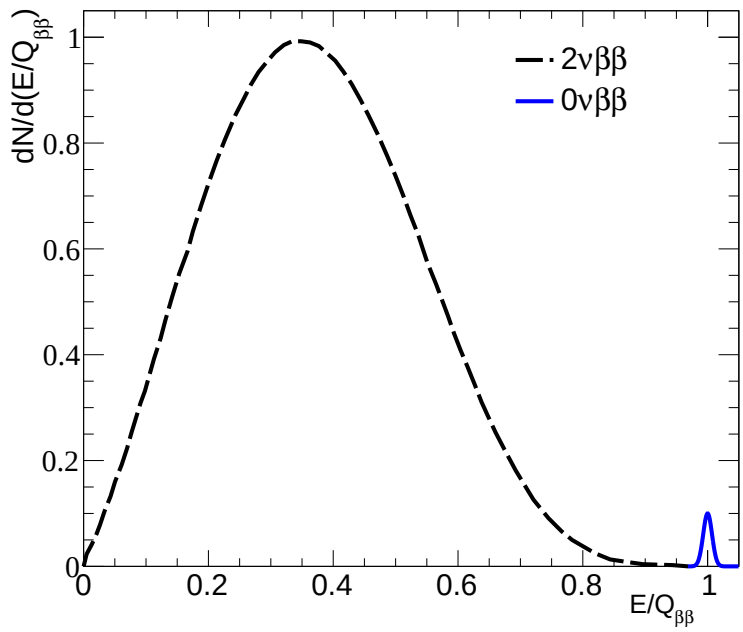

Figure 2. Typical spectrum of a double beta decay (dashed black) and of the neutrinoless double beta decay (blue).

The so-called **neutrinoless double-beta decay** process is sensitive to a quantity denoted effective Majorana mass, $m_{\beta\beta}$:

$$< m_{\beta\beta} > = |\sum_i m_i \; U_{ei}^2 \; e^{i\phi}|. \tag{3}$$

where m_i are the Majorana masses of the individual mass eigenstates and U_{ei} the components of the neutrino mixing matrix.

Equation 3 includes Majorana phases ϕ which affect the measurement of the effective Majorana mass. As discussed in previous lectures, two options are possible for the neutrino mass ordering:

- $m_3 > m_2 > m_1$ called **normal** ordering or hierarchy (NH)
- $m_2 > m_1 > m_3$ called **inverted** ordering or hierarchy (IH)

Figure 3 shows the **dependence of the effective Majorana mass** on the **lightest neutrino mass** for both hierarchies. For NH, there are values of the Majorana phases ϕ that lead to cancellation resulting into negligible values for $m_{\beta\beta}$. The color scale represents the probability distribution of values computed via sampling of the mixing angle and squared mass difference distributions.

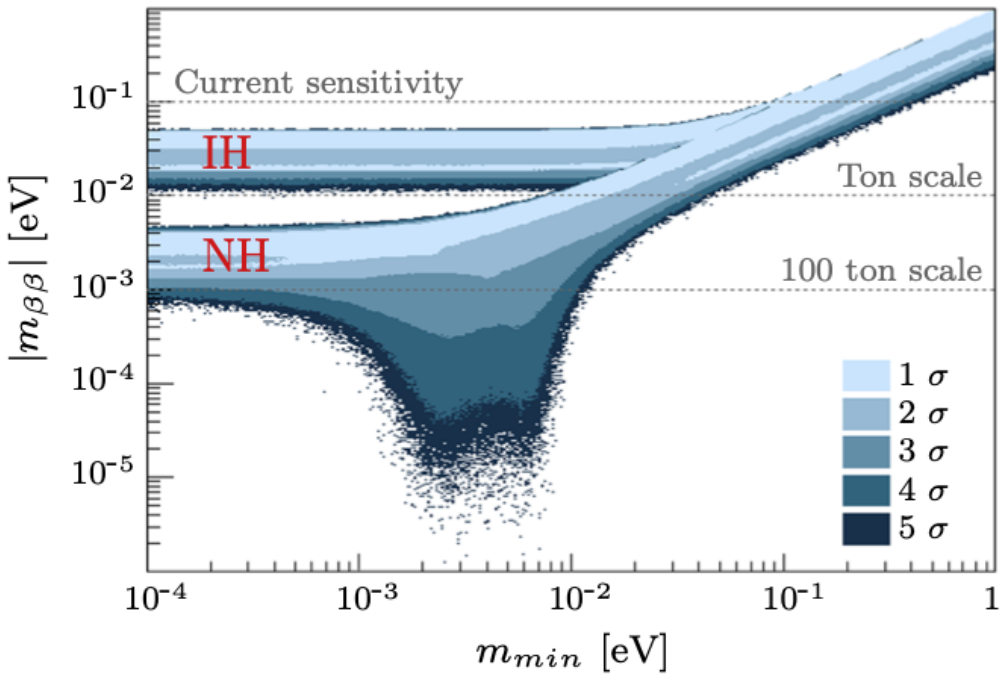

Figure 3. Effective Majorana mass as a function of the lightest neutrino mass showing the normal and inverted hierarchies, NH and IH, respectively. Figure from [3].

1.2. Nuclear physics aspects

Nuclear matrix elements are required to evaluate the decay half-life of the neutrinoless double-beta decay process. For the most common exchange model used in the community (light-neutrino exchange model), the $0\nu\beta\beta$ half-life can be written as [1]:

$$T_{1/2} = (G \cdot |\mathcal{M}|^2 \cdot < m_{\beta\beta} >^2)^{-1} \tag{4}$$

where G is a phase-space factor and $\mathcal{M}$ the matrix element of this nuclear decay process.

The nuclear matrix elements account for the nuclear structure and as they can not be measured separately, they must be **evaluated theoretically**. Due to the many-body nature of the problem, only approximate estimates can be obtained at present time. Such theoretical approaches exits but unfortunately, the results of those **calculations differ** from each other by some factor. This results into a non negligible error to the $0\nu\beta\beta$ measurement. This will be particularly important in the case of a discovery.

Figure 4 shows the values of the matrix elements for some of the common nuclear calculations [4]: the interacting shell model (ISM), quasi-particle random-phase approximation (QRPA Tübingen and QRPA Jyväskyla), interacting boson model (IMB-2), and energy density functional method (EDF).

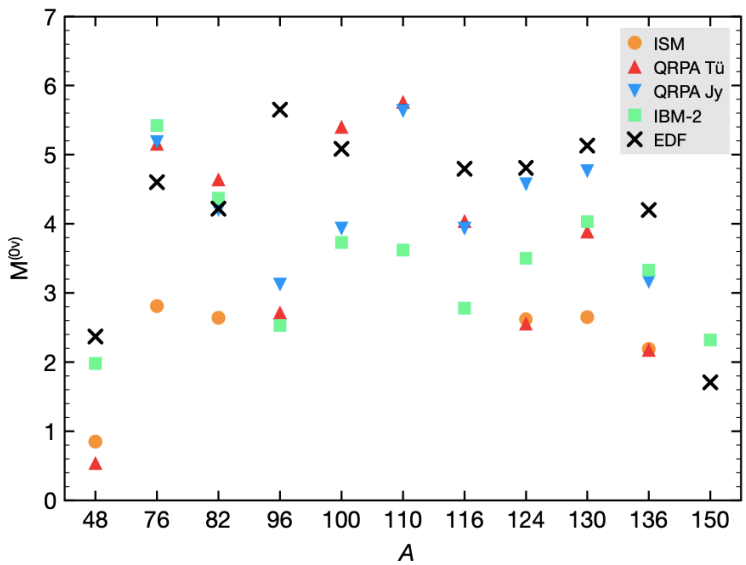

Figure 4. Nuclear matrix elements as function of mass number (A) for the $0\nu\beta\beta$ decay to the ground state as calculated in four different frameworks (see text). Figure from [4].

1.3. Experimental aspects

To measure the two electrons emitted in the decay, mostly **spectroscopy** techniques are used, i.e. looking for a monoenergetic peak. Another option is to use detectors capable of **tracking** and reconstruct the topology of these electrons.

To realize a $0\nu\beta\beta$ experiment, a technology has tobe chosen taking into account the candidate isotopes. Table 1 summarizes properties for the most important isotopes considered for $0\nu\beta\beta$ searches: the **natural abundance** and $Q_{\beta\beta}$ **value**. Note that in total there are 35 $\beta\beta$-decaying isotopes but not all are suitable for an experiment.

Table 1. Summary of parameters for commonly employed $\beta\beta$-decay isotopes. Data from [1].

Isotope	Natural abundance [%]	$Q_{\beta\beta}$ [MeV]
^{48}Ca	0.187	4.263
^{76}Ge	7.8	2.039
^{82}Se	8.7	2.998
^{96}Zr	2.8	3.348
^{100}Mo	9.8	3.035
^{116}Cd	7.5	2.813
^{130}Te	34.08	2.527
^{136}Xe	8.9	2.459
^{150}Nd	5.6	3.371

Candidate $0\nu\beta\beta$-events are searched for in an energy region around the $Q_{\beta\beta}$ for each isotope. The number of events in this region can be written as [1]:

$$N \propto \frac{N_A}{W} \cdot \frac{a \cdot \epsilon \cdot M \cdot t}{T_{1/2}} \tag{5}$$

- N_A is the Avogadro number
- W the molar mass,
- a is the isotopic abundance,
- ϵ the detection efficiency in the signal region,
- M is the mass of the corresponding isotope,
- t the measuring time, and
- $T_{1/2}$ the half life of the isotope.

Isotope abundance or enrichment:

The isotopic abundance enters linearly in equation 5. For the cases where the **natural abundance is relatively large** (for instance ^{130}Te), the natural element can be taken directly. Alternatively, the corresponding element can be **enriched in the isotope of interest**. This however typically results in a significantly larger prize for the target.

Energy resolution:

An excellent energy resolution is a key parameter for these experiments, specially for the detectors using spectroscopy. First of all, a good energy resolution allows to distinguish the $0\nu\beta\beta$ signal from background lines (from **natural radioactivity**) in the spectrum. Furthermore even for a background free experiment, **background is expected from the $2\nu\beta\beta$ process** which's spectrum ends exactly at the position of the $0\nu\beta\beta$-signal (figure 2).

The sensitivity to the $0\nu\beta\beta$ half life [1] depends on various factors:

$$T_{1/2} \propto \begin{cases} a \cdot M \cdot \epsilon \cdot t & \text{background free case,} \\ a \cdot \epsilon \sqrt{\frac{M \cdot t}{B \cdot \Delta E}} & \text{with background} \end{cases} \tag{6}$$

- with B the background index, and
- ΔE the energy resolution.

Energy of Q-value and background:

The Q-value is important for an experiment for two reasons. First, the $0\nu\beta\beta$ half life scales as $\propto Q_{\beta\beta}^5$ (**phase-factor** scaling) giving a significantly larger rate.

The second reason is the background from **natural radioactivity**. Most of the naturally occurring decays are below 2.6 MeV which is the energy of the ^{208}Tl line from the thorium decay chain. As an example, figure 5 shows the measured energy spectrum of EXO-200 including the best fit to the background and its main components.

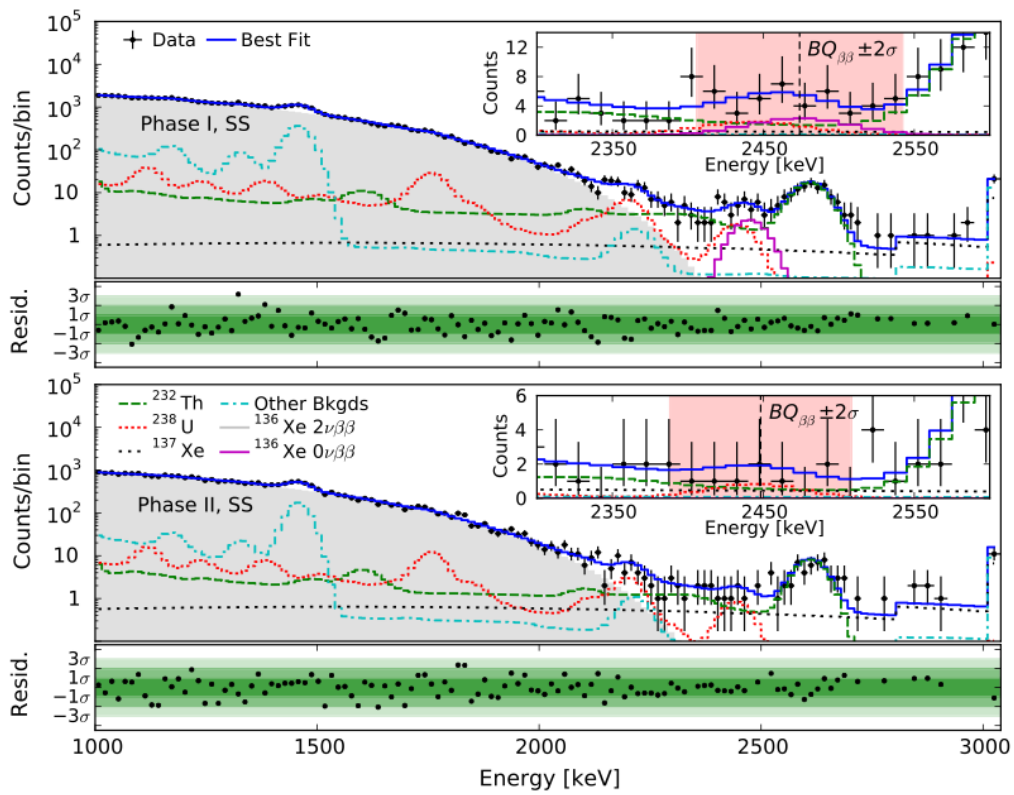

Figure 5. Energy spectrum of selected candidate events together with the best-fit backgrounds and $2\nu\beta\beta$ decays (grey) in the EXO-200 experiment. Figure from [5].

In this case the Q-value is at 2.459 MeV (blue line ^{136}Xe). Both the tail of $2\nu\beta\beta$ (grey area) and contributions from natural radioactivity (uranium and thorium in green and red, respectively) limit the sensitivity of the experiment. Nevertheless, EX0-200 has place some of the most competitive limits on the process half life (see section 1.4.3).

1.4. Current experimental strategies and results

To test the existence of $0\nu\beta\beta$, the isotope of interest needs to be contained in a detector such that the energy deposition by the two electrons can be precisely measured. This section will briefly describe the different experimental strategies which includes detectors made directly out of the material of interest, having the isotope dissolved or bounded in a detector medium and also having the source separated from the detector.

1.4.1. Germanium semiconductors

Germanium detectors combine a high **radio-purity** of the target material with an **excellent energy resolution** around 0.15% for 1 MeV deposited energy. Isotopically enriched crystals are commercially available, increasing from the ^{76}Ge natural abundance of 7.8 % to an enrichment level at $\sim$ 85 %. The typical size of each detector is $\sim (10 - 20)$ kg.

The two electrons deposit their energy in the germanium target ionizing its atoms. An electric field guides electrons/holes to the read out. Specifically, the detectors are of the so-called point-contact type which give a good separation of single and multiple scattering. This is important to suppress any remaining backgrounds.

The **Heidelberg-Moscow** experiment which was running at the LNGS laboratory in Italy between 1992 and 2000, claimed a measurement of the $0\nu\beta\beta$ process. The result was quite controversial in the community and has been tested in the recent GERDA experiment (see below). The half life derived by the Heidelberg-Moscow experiment was $T_{1/2} = 1.5 \times 10^{25}$ y [6].

The GERmanium Detector Array (**GERDA**) experiment searched for $0\nu\beta\beta$ using bare germanium diodes in a liquid argon shield (see figure 6). Due to its excellent energy resolution and its background suppression measures, GERDA performs its search in a

Figure 6. Illustration of the GERDA experiment at LNGS (Italy). A large cryostat filled with liquid argon host the germanium diodes in its center. Figure from the GERDA homepage.

background-free manner achieving a great sensitivity (equation 6). Figure 7 shows the background spectrum of GERDA after all analysis cuts (red). The Q-value at 2.04 MeV

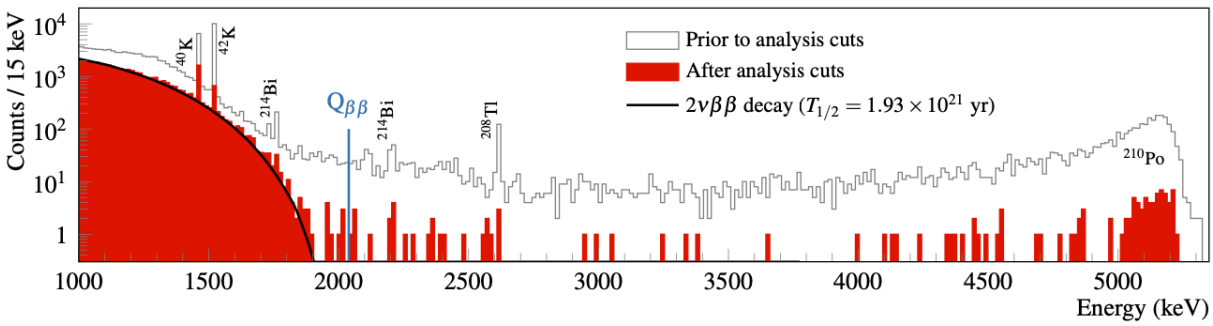

Figure 7. Background spectrum of the GERDA Phase II experiment. The most prominent γ-lines as well as the α population at 5.3 MeV are labelled. Figure from [7].

is marked in blue.

Latest GERDA data [7] using 100 kg× y exposure obtained one of the best results in the field. A limit on the half-life of $0\nu\beta\beta$ decay of ^{76}Ge is set at $T_{1/2} > 1.8 \times 10^{26}$ y at 90% C.L., which coincides with the sensitivity assuming no signal. Note that this value is significantly larger than the signal claim by the Heidelberg-Moscow experiment.

1.4.2. Cryogenic bolometers

Detectors collecting the phonon signal produced in crystals are developed to reach very low thresholds and excellent energy resolutions. Cryogenic bolometers are **operated at ∼mK temperatures** in order to record the tiny temperature increase (typically ∼ 0.1 mK per MeV) induced by the energy deposited by charged particles. This temperature change can be recorded with thermal sensors. Similar to semiconductor detectors, crystalline bolometers can be intrinsically low in radioactivity because of the crystal growth process. However, operating at extremely low temperatures increases the technical difficulty of building and carrying out such experiments.

The Cryogenic Underground Observatory for Rare Events (**CUORE**) located at the LNGS laboratory in Italy, employs $\mathcal{O}(1000)$ TeO_2 crystals to search for $0\nu\beta\beta$ in ^{130}Te. This isotope has the largest natural isotopic abundance of 34.2 % and therefore it is used without enrichment. Each crystal has a size of $5 \times 5 \times 5\,\mathrm{cm}^3$ and weights 750 g giving a total mass of 741 kg. A photograph of the array consisting of 25 towers of 40 crystals each can be seen in figure 8.

In the latest results of COURE from 2020, **no evidence** for $0\nu\beta\beta$ decay was found and an exclusion limit of $T_{1/2} > 3.2 \times 10^{25}$ y was set [8].

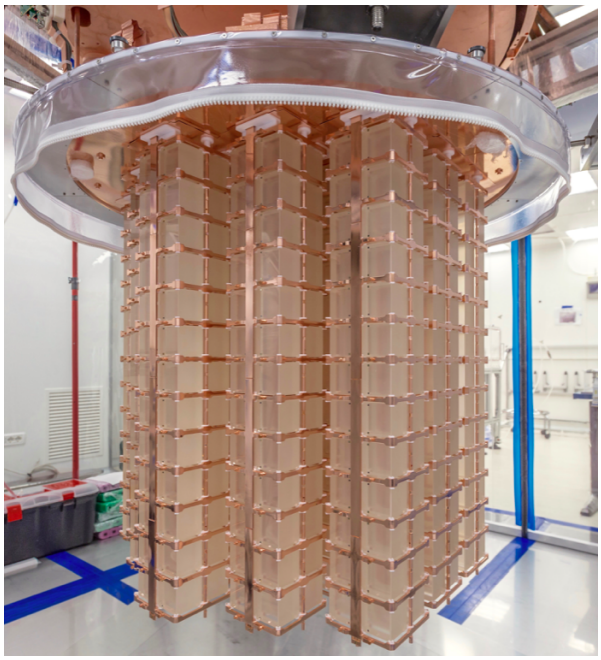

Figure 8. Photograph of the CUORE experiment assembly before it began taking data. Figure from the CUORE collaboration.

1.4.3. Detectors using xenon

Several experiments employ xenon to search for $0\nu\beta\beta$. Although xenon contains naturally $\sim 9\,\%$ of ^{136}Xe, most experiments enrich their xenon to have $(80-90)\,\%$ of ^{136}Xe in the target. Currently **three technologies** are being pursued: dissolving xenon in organic scintillator, using liquified xenon (at $-100°$C) or high pressure xenon.

Organic scintillator loaded with xenon

The KamLAND experiment (discussed in the reactor neutrino lecture) upgraded their instrument by placing an inner balloon with xenon-loaded liquid scintillator [9]. Figure 9 shows this upgraded detector called **KamLAND-Zen**. A central ballon (in purple in the figure) is filled with scintillator loaded with xenon.

In the first phase of the experiment (with 320 kg of enriched xenon) the sensitivity of the experiment was limited due to the contamination of the experiment with a silver isotope ^{110m}Ag. The decay of this isotope which origin is related to the Fukushima reactor accident in 2011, produces a signal exactly at the Q-value of ^{136}Xe. After purification, the experiment managed to reduce significantly the ^{110m}**Ag contamination**. Combining the results from the first and second phases, the experiment obtained a lower limit for the $0\nu\beta\beta$ decay half-life of $T_{1/2} > 1.07 \times 10^{26}$ y at 90% C.L. [10]. Using commonly adopted nuclear matrix element calculations, the corresponding upper limits on the effective Majorana neutrino mass are in the range

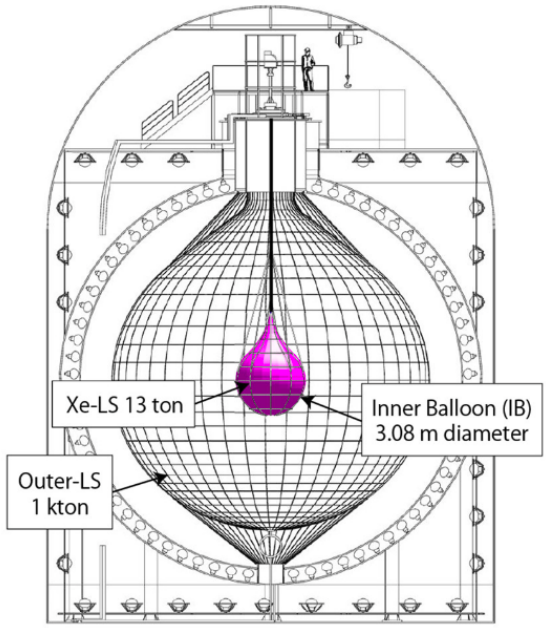

Figure 9. Illustration of the KamLAND-Zen experiment showing in purple the inner balloon which is loaded with xenon. Figure from [9].

$(61 - 165)$ meV.

In a follow-up phase, the KamLAND-Zen Collaboration has completed the installation of a new mini-balloon which is loaded with 750 kg of enriched Xe. Data taking with this experiment is ongoing. While very large sensitivities can be achieved by this experiment due to its **great mass**, the **energy resolution** (of $\sim 7\,\%$ at 1 MeV) is not as good as for crystals. For this reason, in the longer term this experiment could be limited by the background of $2\nu\beta\beta$.

Liquid xenon time-projection-chamber (TPC)

Another option is to employ xenon directly as scintillator. For this purpose and in order to have a large mass in a compact volume, the xenon is **cooled down to** $-100°$**C** until it reaches its liquid phase. Charged particles excite and ionize the liquid xenon. While photons from the de-exitation are recorded using photosensors, the electrons can be collected by applying a drift field. With such TPC detector the position of the events can be determined with great precision. In addition, combining the two signals, **charge and light**, allow to achieve an energy resolution of $\sim 1\,\%$ improving towards experiments like KamLAND-Zen.

The Enriched Xenon Observatory (**EXO-200**) [11] employs a TPC to search for $0\nu\beta\beta$ with a 110 kg of liquid xenon enriched to 80.6 % in ^{136}Xe. In EXO-200, a common cathode separates the liquid xenon TPC in two drift regions of 20 cm length (see figure 10). With an electric field of 380 V/cm the electrons are drifted to the crosses-wire

planes at each anode. The scintillation is recorded by arrays of avalanche photo-diodes located behind the wire planes.

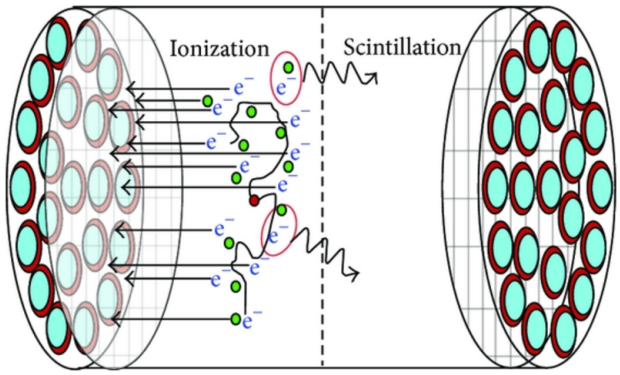

Figure 10. Illustration of the working principle of the EXO-200 detector. Figure from the EXO-200 Collaboration.

EXO-200 is quite a compact detector compared to KamLAN-Zen for instance because of the high density of liquid xenon of $2.9\,\mathrm{g/cm^3}$. EXO has performed several science runs collecting a total exposure of 234.1 kg·y. A combined result from these runs for the $0\nu\beta\beta$ decay half-life is at $T_{1/2} > 5.0 \times 10^{25}$ y at 90% C.L. The collaboration plans on a larger detector (nEXO) which would have a mass of $\sim 5\,\mathrm{t}$ of liquid xenon.

High pressure xenon

Instead of cooling down the xenon, an alternative is to build a high pressure TPC (typically at $\sim 10\,\mathrm{bar}$). A large volume is required to have a mass comparable with the experiment above, but an additional signal feature becomes available. Indeed in the gas phase, the traces of the two electrons can be reconstructed. This allows to suppress background very effectively. A detector of this type has been constructed and operated by the NEXT [12] collaboration at the Laboratorio Subterráneo de Canfranc in the spanish Pyrenees.

1.4.4. Tracking detectors

Until now we have discussed experiments searching for a peak on top of their background spectra. There is however an additional signature which can be used to discriminate double beta decay from background: the **event topology**.

The **NEMO experiment** (at the Modane underground laboratory in France) used exactly the event topology to identify double beta decays of several isotopes. It consisted of a hollow cylinder divided in 20 sectors hosting **thin source foils** from 7 different enriched isotopes. The distribution of the isotopes employed in the detector can be

seen in figure 11 (left). Most of the foils contain ^{100}Mo but also other isotopes were investigated.

Double beta decays in the foils produce two electrons which travel out of the foil into tracking detectors. These are Geiger cells (gaseous medium, showed in green on the right side of figure 11) which provide a three dimensional measurements of the particle track. Charged particles have a curved trajectory caused by a 25 G magnetic field produced by a solenoid surrounding the detector.

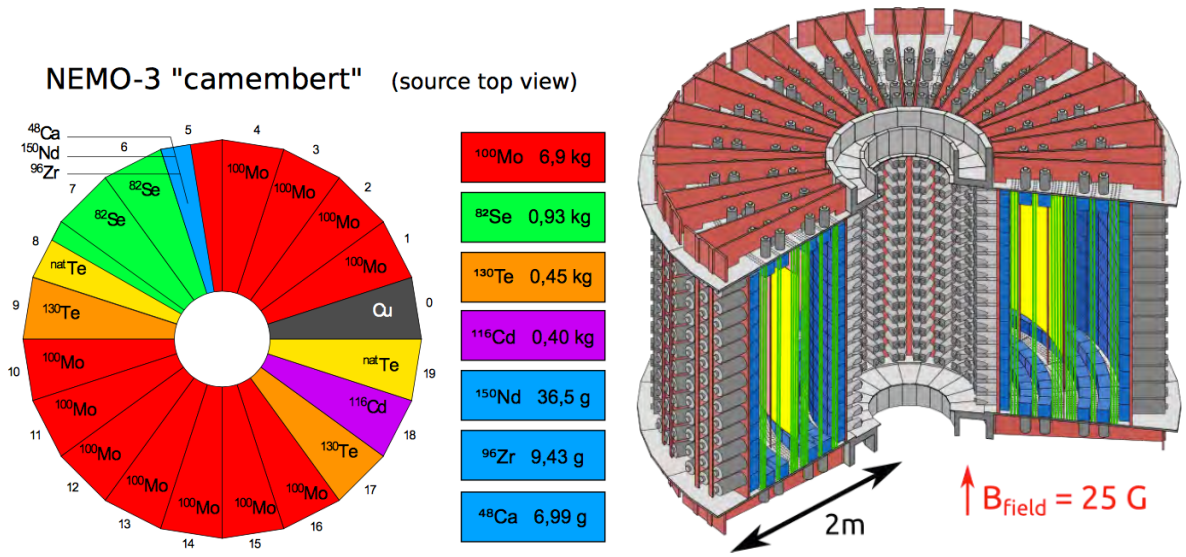

Figure 11. Right: distribution of isotopes in the NEMO experiment. Left: Schemetic representation of the experiment including the sources (yellow), the tracker (green) and the calorimeter (blue). Figures from the NEMO homepage.

The tracking chamber is inclosed on calorimeter walls (scintillator crystals, in blue in the figure) which record the energy deposition by the emitted electrons and provide also timing information.

NEMO-3 has placed limits on the $0\nu\beta\beta$ half life for **various isotopes**. The most sensitive search is performed with ^{100}Mo as it makes up most of the target mass in the experiment (see figure 11). For this isotope, a lower limit of the half life is placed at $T_{1/2} > 1.1 \times 10^{24}$ y [13]. Limits are placed also for ^{48}Ca, ^{82}Se, ^{96}Zr, ^{116}Cd, ^{130}Te and ^{150}Nd (see table 2).

1.5. Status of experimental results

In the sections above, we have reviewed some of the technologies employed to search for the rare $0\nu\beta\beta$ decay. We learn that key properties of a detector are a good energy resolution and a low background. Figure 12 summarizes the values of these two parameters for various past, current and future experiments.

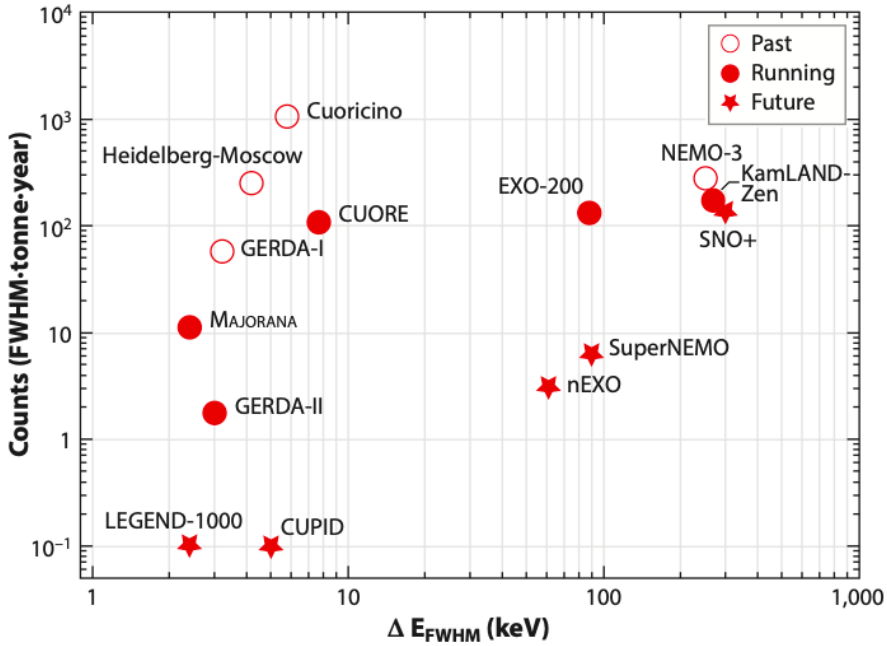

Figure 12. Background index as function of the energy resolution for a selection of past, current and future experiments. Figure from [1].

It can be seen that **germanium detectors and bolometers** have superb resolutions and low background index and therefore future large detectors (like Legend and CUPID) are being planned. Note however, that the scalability of this technology is not trivial. Indeed, technologies able to scale up to a large mass (order of a ton) are most interesting for the future.

Table 2 summarizes a selection of results for recent $0\nu\beta\beta$ including the limit on the half life but also the effective neutrino mass range that is excluded.

Table 2. Summary of results of $T_{1/2}$ and $m_{\beta\beta}$ for a selection of experiments. Data from [1][7][8] & [11].

Isotope	$T_{1/2}$ [$\times 10^{25}$ y]	$m_{\beta\beta}$ [eV]	Experiment
^{76}Ge	> 18	$< (0.079 - 0.18)$	GERDA
^{82}Se	$> 3.6 \times 10^{-2}$	$< (0.89 - 2.43)$	NEMO-3
^{96}Zr	$> 9.2 \times 10^{-4}$	$< (7.2 - 19.5)$	NEMO-3
^{100}Mo	$> 1.1 \times 10^{-1}$	$< (0.33 - 0.62)$	NEMO-3
^{130}Te	> 3.2	$< (0.075 - 0.35)$	CUORE
^{136}Xe	> 10.7	$< (0.061 - 0.165)$	KamLAND-Zen
^{136}Xe	> 3.5	$< (0.093 - 0.29)$	EXO-200
^{150}Nd	$> 2.0 \times 10^{-3}$	$< (1.6 - 5.3)$	NEMO-3

Figure 13 compares the $0\nu\beta\beta$ sensitivities and half life limits from GERDA, KamKAND-Zen and the EXO-200 experiments. The figure includes the observation claim in ^{76}Ge which is meanwhile strongly disfavoured by the GERDA results. The

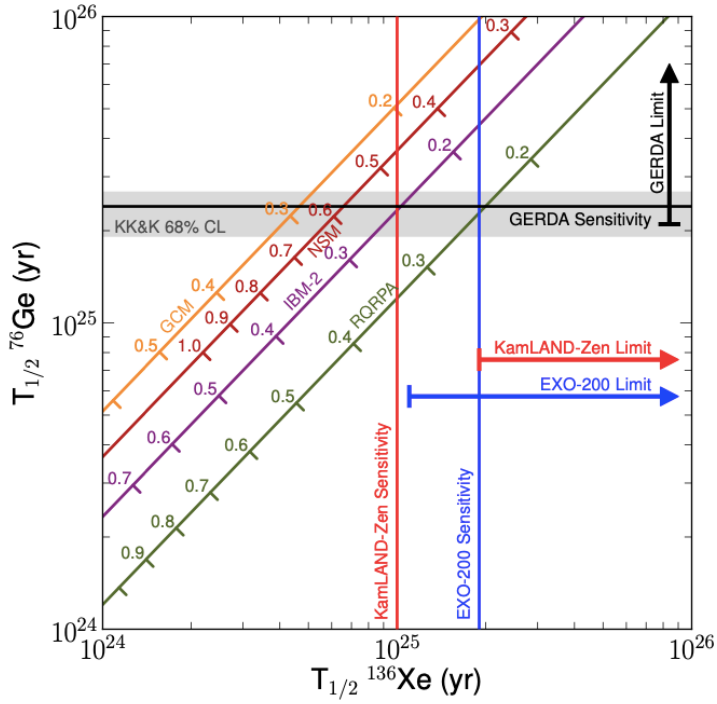

Figure 13. Comparison of germanium and xenon results from different experiment including their sensitivity and the actual limits. Figure from [14].

diagonal lines are derived from several nuclear matrix element calculations and phase space factors to allow the comparison between the two isotopes. Tick marks along these lines indicate the associated effective neutrino mass in eV.

1.6. Summary

In this lecture, we reviewed the experimental search for lepton number violation searching for $0\nu\beta\beta$ decays. We discussed the main factors affecting the sensitivity of these experiments and also the main technologies being developed for such measurement.

References

[1] M. J. Dolinski, A. W. P. Poon, and W. Rodejohann, "Neutrinoless Double-Beta Decay: Status and Prospects," *Ann. Rev. Nucl. Part. Sci.* **69** (2019) 219, `arXiv:1902.04097`.

[2] M. Goeppert-Mayer, "Double beta-disintegration," *Phys. Rev.* **48** (1935) 512.

[3] G. Benato, "Effective Majorana Mass and Neutrinoless Double Beta Decay," *Eur. Phys. J. C* **75** no. 11, (2015) 563, `arXiv:1510.01089`.

[4] J. J. Gómez-Cadenas and J. Martín-Albo, "Phenomenology of neutrinoless double beta decay," *PoS* **GSSI14** (2015) 004, `arXiv:1502.00581`.

[5] **EXO** Collaboration, J. B. Albert *et al.*, "Search for Neutrinoless Double-Beta Decay with the Upgraded EXO-200 Detector," *Phys. Rev. Lett.* **120** no. 7, (2018) 072701, arXiv:1707.08707.

[6] H. V. Klapdor-Kleingrothaus, A. Dietz, H. L. Harney, and I. V. Krivosheina, "Evidence for neutrinoless double beta decay," *Mod. Phys. Lett. A* **16** (2001) 2409, arXiv:hep-ph/0201231.

[7] **GERDA** Collaboration, M. Agostini *et al.*, "Final Results of GERDA on the Search for Neutrinoless Double-β Decay," *Phys. Rev. Lett.* **125** no. 25, (2020) 252502, arXiv:2009.06079.

[8] **CUORE** Collaboration, D. Q. Adams *et al.*, "Improved Limit on Neutrinoless Double-Beta Decay in ^{130}Te with CUORE," *Phys. Rev. Lett.* **124** no. 12, (2020) 122501, arXiv:1912.10966.

[9] I. Shimizu and M. Chen, "Double beta decay experiments with loaded liquid scintillator," *Frontiers in Physics* **7** (2019) 33.

[10] **KamLAND-Zen** Collaboration, A. Gando *et al.*, "Search for Majorana Neutrinos near the Inverted Mass Hierarchy Region with KamLAND-Zen," *Phys. Rev. Lett.* **117** no. 8, (2016) 082503, arXiv:1605.02889. [Addendum: Phys.Rev.Lett. 117, 109903 (2016)].

[11] **EXO-200** Collaboration, G. Anton *et al.*, "Search for Neutrinoless Double-β Decay with the Complete EXO-200 Dataset," *Phys. Rev. Lett.* **123** no. 16, (2019) 161802, arXiv:1906.02723.

[12] **NEXT** Collaboration, P. Ferrario *et al.*, "First proof of topological signature in the high pressure xenon gas TPC with electroluminescence amplification for the NEXT experiment," *JHEP* **01** (2016) 104, arXiv:1507.05902.

[13] **NEMO-3** Collaboration, R. Arnold *et al.*, "Results of the search for neutrinoless double-β decay in ^{100}Mo with the NEMO-3 experiment," *Phys. Rev. D* **92** no. 7, (2015) 072011, arXiv:1506.05825.

[14] **EXO-200** Collaboration, J. B. Albert *et al.*, "Search for Majorana neutrinos with the first two years of EXO-200 data," *Nature* **510** (2014) 229, arXiv:1402.6956.